Inorg. Chem. **2007**, *46*, 2929–2942

Synthesis and Catalytic Properties in Olefin Epoxidation of Novel Iron(II) Complexes with Pyridine-Containing Macrocycles Bearing an Aminopropyl Pendant Arm

Sonia Taktak, Wanhua Ye, Aida M. Herrera, and Elena V. Rybak-Akimova*

Department of Chemistry, Tufts University, Medford, Massachusetts 02155

Received January 18, 2007

Three novel iron(II) complexes with pyridine-containing macrocycles bearing an aminopropyl pendant arm were synthesized and characterized. Crystal structures of two of the complexes revealed high-spin iron(II) centers coordinated to the five ligand nitrogen atoms with no coordination of either the solvent molecules or anions, resulting in an unusual square-pyramidal geometry. Related tetradentate ligand CRH formed a low-spin iron(II) complex (meso form was structurally characterized) with a planar arrangement of the four nitrogen atoms from the macrocycle and two axial acetonitrile molecules. Similarly to the corresponding nickel and copper complexes of the pentadentate ligands, the protonation of the amino group on the ligand arm in iron(II) complexes was found to be reversible. Spectral changes and magnetic susceptibility measurements indicated that a change in the geometry and spin state of the metal center is associated with this acid–base process. In the presence of noncoordinating acids (e.g., triflic acid), these complexes, as well as their nonmethylated analogue, can efficiently catalyze the epoxidation of cyclooctene and 1-decene under mild conditions, using hydrogen peroxide as the oxidant. However, in the deprotonated form or in the presence of coordinating acids like HCl, no epoxidation occurs.

Introduction

In the search for nontoxic, efficient, and synthetically accessible oxidation catalysts, biomimetic non-heme iron complexes show considerable promise.[1−4] The ability of biological catalysts to activate dioxygen and hydrogen peroxide is of particular interest because water is the only oxidant-derived byproduct in these systems. In order to understand and mimic oxygen and peroxide activation by non-heme iron enzymes, critical components of the iron coordination sphere that are essential for catalytic activity need to be identified. In this work, we developed novel mononuclear iron(II) complexes that catalyze olefin epoxidation with H_2O_2 under mild conditions and resemble the coordination geometry of the active site of iron bleomycin. Our studies focused on the role of tetragonal-pyramidal geometry in oxygen and peroxide activation by non-heme iron centers.

Bleomycin (BLM), an antibiotic and anticancer drug, mediates oxidative DNA degradation in the presence of oxygen species and iron as cofactors.[5−10] The unique redox reactivity of FeBLM resembles in many respects oxygen and peroxide activation with heme proteins. Fe^{II}BLM reacts with oxygen to form activated bleomycin (ABLM), which is a low-spin end-on $Fe^{III}OOH$ complex (Chart 1).[11−13] In addition to DNA cleavage,[9,11,13] ABLM is able to catalyze oxidation reactions of small molecules, such as olefin epoxidations and aromatic hydroxylations.[8,14,15]

* To whom correspondence should be addressed. E-mail: elena.rybak-akimova@tufts.edu.

(1) Backvall, J.-E., Ed. *Modern Oxidation Methods*; Wiley-VCH: Weinheim, Germany, 2004.
(2) Costas, M.; Mehn, M. P.; Jensen, M. P.; Que, L., Jr. *Chem. Rev.* **2004**, *104*, 939−986.
(3) Lane, B. S.; Burgess, K. *Chem. Rev.* **2003**, *103*, 2457−2473.
(4) Meunier, B., Ed. *Metal−Oxo and Metal−Peroxo Species in Catalytic Oxidations*; Structure and Bonding, Vol. 97; Springer: Berlin, 2000.
(5) Sausville, E. A.; Peisach, J.; Horwitz, S. B. *Biochemistry* **1978**, *17*, 2740−2746.
(6) Burger, R. M. *Chem. Rev.* **1998**, *98*, 1153−1169.
(7) Feig, A. L.; Lippard, S. J. *Chem. Rev.* **1994**, *94*, 759−805.
(8) Hecht, S. M. *Acc. Chem. Res.* **1986**, *19*, 383−391.
(9) Stubbe, J.; Kozarich, J. W.; Wu, W.; Vanderwall, D. E. *Acc. Chem. Res.* **1996**, *29*, 322−330.
(10) Stubbe, J.; Kozarich, J. W. *Chem. Rev.* **1987**, *87*, 1107−1136.
(11) Burger, R. M. In *Metal−Oxo and Metal−Peroxo Species in Catalytic Oxidations*; Springer: Berlin, 2000; Vol. 97, pp 287−303.
(12) Solomon, E. I.; Brunold, T. C.; Davis, M. I.; Kemsley, J. N.; Lee, S.-K.; Lehnert, N.; Neese, F.; Skulan, A. J.; Yang, Y.-S.; Zhou, J. *Chem. Rev.* **2000**, *100*, 235−349.
(13) Decker, A.; Chow, M. S.; Kemsley, J. N.; Lehnert, N.; Solomon, E. I. *J. Am. Chem. Soc.* **2006**, *128*, 4719−4733.

10.1021/ic070094e CCC: $37.00
Published on Web 03/03/2007

Chart 1. Iron Coordination Sphere in ABLM

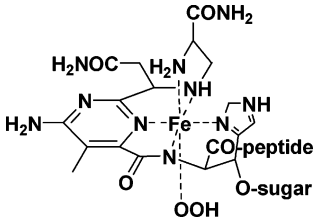

Spectroscopic methods showed that high-spin iron(II) coordinates in a pseudo-square-pyramidal geometry, with pyrimidine and imidazole nitrogen, deprotonated amide, and the secondary amine of the β-aminoalanine residue as equatorial donors.[16] The nature of the axial ligand has long been debated; the candidates were the primary amino group of β-aminoalanine[17] and the carbamoyl group from the mannose sugar.[18,19] Convincing evidence in favor of amino group coordination in Fe^{II}BLM has been obtained by magnetic circular dichroism spectroscopy[20] and NMR of paramagnetic Fe^{II}BLM.[21] The same coordination mode has been established for both (Co^{III}OOH)BLM and its adduct with an oligonucleotide.[22−24] Recent X-ray absorption near-edge structure results are consistent with the primary amine occupying the fifth position and the sugar oxygen atom coordinated in the sixth position.[25] Even though the nature of the axial ligands in Fe^{II}BLM now appears to be firmly established, at least one of these ligands (most likely, the mannose oxygen) has to dissociate in order for the dioxygen molecule to bind to the iron center. It is also possible that additional rearrangements in the iron coordination sphere occur in the course of oxygen coordination.[26]

Several iron(II) complexes bearing pentadentate N5 ligands have been synthesized to model Fe^{II}BLM, with the goal of achieving an understanding of electronic and structural features that control the "heme-like" redox reactivity of mononuclear non-heme complexes. Complexes of the amidate-based ligands PMAH and their analogues have been found to react with dioxygen and promote DNA cleavage as well as olefin epoxidation.[27−30] Iron(II) complexes of pentadentate aminopyridine ligands are more numerous and include systems containing two to five pyridines.[31−43] In most cases, the geometry around the iron center is octahedral, with five nitrogens provided by the pentadentate ligand and one site occupied by a solvent molecule or an anion. The spin state of these ferrous complexes can generally be tuned by changing the nature of this sixth monodentate ligand. These systems have been shown to react with hydrogen peroxide to form metastable Fe^{III}OOH intermediates and in some cases to catalyze oxidation reactions. However, these ligands, most of which had open-chain topology, did not fix all donors in a well-defined square-planar or square-pyramidal geometry about iron. As a result, the exact coordination environment around the metal center in active oxidants remains unclear in most cases. In order to systematically address the potential significance and the role of the fifth donor that may coordinate to a square-planar FeN_4 scaffold, we designed pyridine-containing macrocyclic ligands L1−L3 bearing an aminopropyl pendant arm (Chart 2). Equatorial coordination of four nitrogen atoms in these systems is constrained by the ring, while the arm is flexible and its coordination in the axial position can be tuned by simple acid−base additions.

The synthesis of the ligands and the preparation of their nickel(II) and copper(II) complexes were previously reported by our group.[44] For both metal ions, the geometry around

(14) Heimbrook, D. C.; Carr, S. A.; Mentzer, M. A.; Long, E. C.; Hecht, S. M. *Inorg. Chem.* **1987**, *26*, 3835−3836.
(15) Murugesan, N.; Hecht, S. M. *J. Am. Chem. Soc.* **1985**, *107*, 493−500.
(16) Itaka, Y.; Nakamura, H.; Nakatani, T.; Muraoka, Y.; Fujii, A.; Takita, T.; Umezawa, H. *J. Antibiot.* **1978**, *31*, 1070−1072.
(17) Sugiura, Y. *J. Am. Chem. Soc.* **1980**, *102*, 5216−5221.
(18) Akkerman, M. A. J.; Neijman, E. W. J. F.; Wijmenga, S. S.; Hilbers, C. W.; Bermel, W. *J. Am. Chem. Soc.* **1990**, *112*, 7462−7474.
(19) Oppenheimer, N. J.; Chang, C.; Chang, L.-H.; Ehrenfeld, G.; Rodriguez, L. O.; Hecht, S. M. *J. Biol. Chem.* **1982**, *257*, 1606−1609.
(20) Loeb, K. E.; Zaleski, J. M.; Hess, C. D.; Hecht, S. M.; Solomon, E. I. *J. Am. Chem. Soc.* **1998**, *120*, 1249−1259.
(21) Lehmann, T. E.; Ming, L.-J.; Rosen, M.; Que, L., Jr. *Biochemistry* **1997**, *36*, 2807−2816.
(22) Wu, W.; Vanderwall, D. E.; Turner, C. J.; Kozarich, J. W.; Stubbe, J. *J. Am. Chem. Soc.* **1996**, *118*, 1281−1294.
(23) Wu, W.; Vanderwall, D. E.; Teramoto, S.; Lui, S. M.; Hoehn, S. T.; Tang, X.-J.; Turner, C. J.; Boger, D. L.; Kozarich, J. W.; Stubbe, J. *J. Am. Chem. Soc.* **1998**, *120*, 2239−2250.
(24) Wu, W.; Vanderwall, D. E.; Lui, S. M.; Tang, X.-J.; Turner, C. J.; Kozarich, J. W.; Stubbe, J. *J. Am. Chem. Soc.* **1996**, *118*, 1268−1280.
(25) Smolentsev, G.; Soldatov, A. V.; Wasinger, E. C.; Solomon, E. I. *Inorg. Chem.* **2004**, *43*, 1825−1827.
(26) Wu, Y.-D.; Houk, K. N.; Valentine, J. S.; Nam, W. *Inorg. Chem.* **1992**, *31*, 718−720.
(27) Nguyen, C.; Guajardo, R. J.; Mascharak, P. K. *Inorg. Chem.* **1996**, *35*, 6273−6281.
(28) Loeb, K. E.; Zaleski, J. M.; Westre, T. E.; Guajardo, R. J.; Mascharak, P. K.; Hedman, B.; Hodgson, K. O.; Solomon, E. I. *J. Am. Chem. Soc.* **1995**, *117*, 4545−4561.
(29) Guajardo, R. J.; Chavez, F.; Farinas, E. T.; Mascharak, P. K. *J. Am. Chem. Soc.* **1995**, *117*, 3883−3884.
(30) Guajardo, R. J.; Hudson, S. E.; Brown, S. J.; Mascharak, P. K. *J. Am. Chem. Soc.* **1993**, *115*, 7971−7977.
(31) Spiccia, L.; Fallon, G. D.; Grannas, M. J.; Nichols, P. J.; Tiekink, E. R. T. *Inorg. Chim. Acta* **1998**, *279*, 192−199.
(32) Roelfes, G.; Vrajmasu, V.; Chen, K.; Ho, R. Y. N.; Rohde, J. U.; Zondervan, C.; la Crois, R. M.; Schudde, E. P.; Lutz, M.; Spek, A. L.; Hage, R.; Feringa, B. L.; Münck, E.; Que, L., Jr. *Inorg. Chem.* **2003**, *42*, 2639−2653.
(33) Hazell, A.; McKenzie, C. J.; Nielsen, L. P.; Schindler, S.; Weitzer, M. *Dalton Trans.* **2002**, 310−317.
(34) Balland, V.; Banse, F.; Anxolabehere-Mallart, E.; Ghiladi, M.; Mattioli, T. A.; Philouze, C.; Blondin, G.; Girerd, J. J. *Inorg. Chem.* **2003**, *42*, 2470−2477.
(35) Mialane, P.; Nivorojkine, A.; Pratviel, G.; Azema, L.; Slany, M.; Godde, F.; Simaan, A.; Banse, F.; Kargar-Grisel, T.; Bouchoux, G.; Sainton, J.; Horner, O.; Guilhem, J.; Tchertanova, L.; Meunier, B.; Girerd, J. J. *Inorg. Chem.* **1999**, *38*, 1085−1092.
(36) Bernal, I.; Jensen, I. M.; Jensen, K. B.; McKenzie, C. J.; Toftlund, H.; Tuchagues, J. P. *J. Chem. Soc., Dalton Trans.* **1995**, 3667−3675.
(37) Machkour, A.; Mandon, D.; Lachkar, M.; Welter, R. *Eur. J. Inorg. Chem.* **2005**, 158−161.
(38) van den Heuvel, M.; van den Berg, T. A.; Kellogg, R. M.; Choma, C. T.; Feringa, B. L. *J. Org. Chem.* **2004**, *69*, 250−262.
(39) Roelfes, G.; Lubben, M.; Hage, R.; Que, L., Jr.; Feringa, B. L. *Chem. Eur. J.* **2000**, *6*, 2152−2159.
(40) Roelfes, G.; Lubben, M.; Chen, K.; Ho, R. Y. N.; Meetsma, A.; Genseberger, S.; Hermant, R. M.; Hage, R.; Mandal, S. K.; Young, V. G.; Zang, Y.; Kooijman, H.; Spek, A. L.; Que, L., Jr.; Feringa, B. L. *Inorg. Chem.* **1999**, *38*, 1929−1936.
(41) Lubben, M.; Meetsma, A.; Wilkinson, E. C.; Feringa, B.; Que, L., Jr. *Angew. Chem., Int. Ed.* **1995**, *34*, 1512−1514.
(42) Goldsmith, C. R.; Jonas, R. T.; Cole, A. P.; Stack, T. D. P. *Inorg. Chem.* **2002**, *41*, 4642−4652.
(43) de Vries, M. E.; LaCrois, R. M.; Roelfes, G.; Kooijman, H.; Spek, A. L.; Hage, R.; Feringa, B. L. *Chem. Commun.* **1997**, 1549−1550.
(44) Herrera, A. M.; Staples, R. J.; Kryatov, S. V.; Nazarenko, A. Y.; Rybak-Akimova, E. V. *Dalton Trans.* **2003**, 846−856.

Chart 2. Ligands Used in This Work

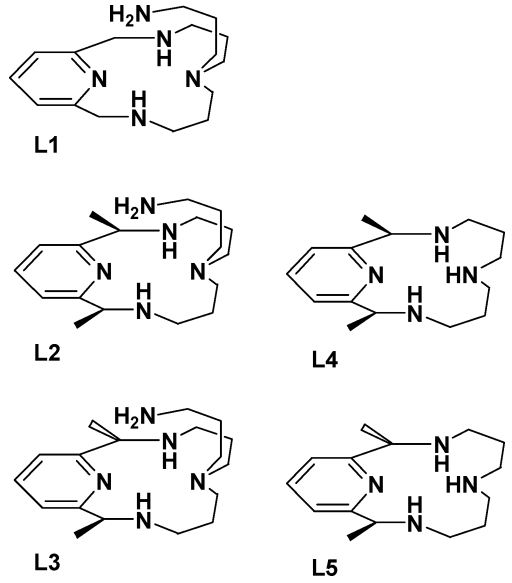

the metal was square-pyramidal, and reversible protonation of the amine on the ligand arm resulted in a change in the geometry around the metal. To the extent of our knowledge, protonation-induced dissociation of the axial ligand incorporated in the pendant arm is unprecedented in non-heme iron chemistry. In the present paper, these ligands were used to prepare the corresponding iron(II) complexes **1**−**3** (Scheme 1). We report that reversible protonation of the pendant arm regulates the catalytic activity of complexes **1**−**3** in olefin epoxidation with H_2O_2 and compare the structure and properties of iron(II) complexes with the pentadentate ligands L1−L3 to the analogous complexes with the tetradentate ligand CRH (L4 and L5, Chart 2).

Experimental Section

General Considerations. All reagents were obtained from commercially available sources and used without further purification, unless otherwise noted. The pentadentate ligands (L1−L3) were prepared as described elsewhere.[44] The tetradentate ligands L4 and L5 were synthesized using a published procedure.[45] $Fe(CH_3CN)_2{\cdot}2CF_3SO_3$ was prepared from $FeCl_2$ and $CF_3SO_3SiMe_3$ in acetonitrile following an unpublished procedure provided by Dr. Miquel Costas and Prof. Lawrence Que, Jr. (University of Minnesota). UV−vis spectra were acquired on a Jasco V-570 spectrophotometer. Gas chromatography (GC) analyses were performed on a Hewlett-Packard 5890 GC instrument equipped with a flame ionization detector and HP *Chemstation 6.01* software. Cyclic voltammetry measurements were carried out using a CH Instruments model 830 electrochemical analyzer. Electrospray mass spectra were recorded on a Finigan LTQ mass spectrometer in the positive ion detection mode. NMR spectra were acquired using a Bruker DPX-300 spectrometer. Elemental analyses were performed by Schwarzkopf Microanalytical Laboratory, Inc. (Woodside, NY).

[Fe(L1)](CF$_3$SO$_3$)$_2$ (1). $Fe(CF_3SO_3)_2{\cdot}2CH_3CN$ (94 mg, 0.216 mmol) dissolved in 5 mL of dry methanol was added to a solution of L1 (70 mg, 0.240 mmol) in 6 mL of dry methanol under an argon atmosphere. Upon mixing, the solution turned green. The mixture was slowly added to a large volume of ether. The desired white/greenish powder of **1** precipitated overnight. Yield: 74 mg (53%). ES-MS(+) (CH_3CN): *m*/*z* 496.3 ($\{[Fe(L1)](CF_3SO_3)\}^+$, 100%), 173.6 ($\{[Fe(L1)]\}^{2+}$, 34%). Anal. Calcd (found) for $C_{18}H_{29}N_5FeO_6F_6S_2$: C, 33.50 (33.91); H, 4.53 (4.62); N, 10.85 (10.81); Fe, 8.65 (8.13).

[Fe(L2)](CF$_3$SO$_3$)$_2$ (2) and [Fe(L2)](ClO$_4$)$_2$ (2′). $Fe(CF_3SO_3)_2{\cdot}2CH_3CN$ (61 mg, 0.140 mmol) dissolved in 1.5 mL of dry acetonitrile was added to a solution of L2 (50 mg, 0.156 mmol) in 1.5 mL of dry methanol under an argon atmosphere. Upon mixing, the solution turned pale blue/green. Colorless crystals were obtained after 2 days by vapor diffusion of diethyl ether into this solution. Yield: 76 mg (80%). ES-MS(+) (CH_3CN): *m*/*z* 524.2 ($\{[Fe(L2)](CF_3SO_3)\}^+$, 100%), 187.6 ($\{[Fe(L2)]\}^{2+}$, 83%). Anal. Calcd (found) for $C_{20}H_{33}N_5FeO_6F_6S_2$: C, 35.67 (34.75); H, 4.94 (5.00); N, 10.40 (10.14); Fe, 8.29 (8.31).

The perchlorate salt of **2** can be prepared by following the same procedure but using $Fe(ClO_4)_2{\cdot}6H_2O$ and L2 as the starting materials. Colorless crystals of **2′** suitable for X-ray diffraction analysis were obtained after 2 days by vapor diffusion of diethyl ether into the reaction mixture. ES-MS(+) (CH_3CN): *m*/*z* 474.2 ($\{[Fe(L2)](ClO_4)\}^+$, 48%), 187.6 ($\{[Fe(L2)]\}^{2+}$, 83%). ***Caution!*** *Perchlorate salts of metal complexes with organic ligands are potentially explosive. Only small amounts of material should be prepared, and these should be handled with great caution.*

[Fe(L3)](CF$_3$SO$_3$)$_2$ (3). $Fe(CF_3SO_3)_2{\cdot}2CH_3CN$ (62 mg, 0.142 mmol) dissolved in 2.0 mL of dry acetonitrile was added to a solution of L3 (55% L3, 45% L4; 50 mg, 0.156 mmol) in 2.0 mL of dry methanol under an argon atmosphere. Upon mixing, the solution turned pale green. A white solid was obtained after 2 days by vapor diffusion of diethyl ether into this solution. Pale-yellow crystals suitable for X-ray diffraction analysis were obtained after slow evaporation of the solvent from an acetonitrile solution of **3**. Yield: 54 mg (57%). ES-MS(+) (CH_3CN): *m*/*z* 524.2 ($\{[Fe(L3)](CF_3SO_3)\}^+$, 100%), 187.6 ($\{[Fe(L3)]\}^{2+}$, 44%).

[Fe(L4)(CH$_3$CN)$_2$](CF$_3$SO$_3$)$_2$ (4). $Fe(CF_3SO_3)_2{\cdot}2CH_3CN$ (149 mg, 0.343 mmol) dissolved in 3 mL of dry acetonitrile was added to a solution of L4 (67% L4, 33% L5−100 mg, 0.381 mmol) in 3 mL of dry methanol under an argon atmosphere. Upon mixing, the solution turned red. Dark-red crystals were obtained after a few days by vapor diffusion of diethyl ether into this solution. Yield: 184 mg (77%). UV−vis [270−800 nm, CH_3CN; λ_{max}, nm (ϵ, L mol^{-1} cm^{-1})]: 370 (sh, 2660), 390 (3120), 526 (120). ES-MS(+) (CH_3CN): *m*/*z* 467.2 ($\{[Fe(L4)](CF_3SO_3)\}^+$, 100%), 179.6 ($\{[Fe(L4)(CH_3CN)]\}^{2+}$, 20%). Anal. Calcd (found) for $C_{19}H_{29}N_5FeO_6F_6S_2$: C, 34.71 (34.91); H, 4.45 (4.57); N, 10.65 (10.63); Fe, 8.49 (8.34). ^{1}H NMR spectroscopy of the pure L4 isomer (δ, ppm in $CDCl_3$): 1.40 (6H, d), 1.65−1.92 (4H, m), 2.31−2.85 (8H, m), 3.76 (2H, quartet), 7.01 (2H, d), 7.56 (1H, t).

Crystals suitable for X-ray diffraction analysis were obtained using a similar procedure starting with a pure L4 isomer. $Fe(CF_3SO_3)_2{\cdot}2CH_3CN$ (121 mg, 0.277 mmol) dissolved in 1 mL of dry acetonitrile was added to a solution of L4 (86 mg, 0.328 mmol) in 0.5 mL of dry methanol under an argon atmosphere. Upon mixing, the solution turned red. Dark-red crystals suitable for X-ray diffraction analysis were obtained after a few days by vapor diffusion of diethyl ether into this solution. Yield: 110 mg (57%).

Synthesis of [Fe(L5)(CH$_3$CN)$_2$](CF$_3$SO$_3$)$_2$ (5). Complex **5** was prepared following the same procedure as that described above for complex **4**. $Fe(CF_3SO_3)_2{\cdot}2CH_3CN$ (149 mg, 0.343 mmol) dissolved in 3 mL of dry acetonitrile was added to a solution of L5 (80% L5, 20% L4; 100 mg, 0.381 mmol) in 3 mL of dry methanol under

(45) Karn, J. L.; Busch, D. H. *Inorg. Chem.* **1969**, *8*, 1149−1153.

Scheme 1. Synthesis of Complexes **1**−**3**

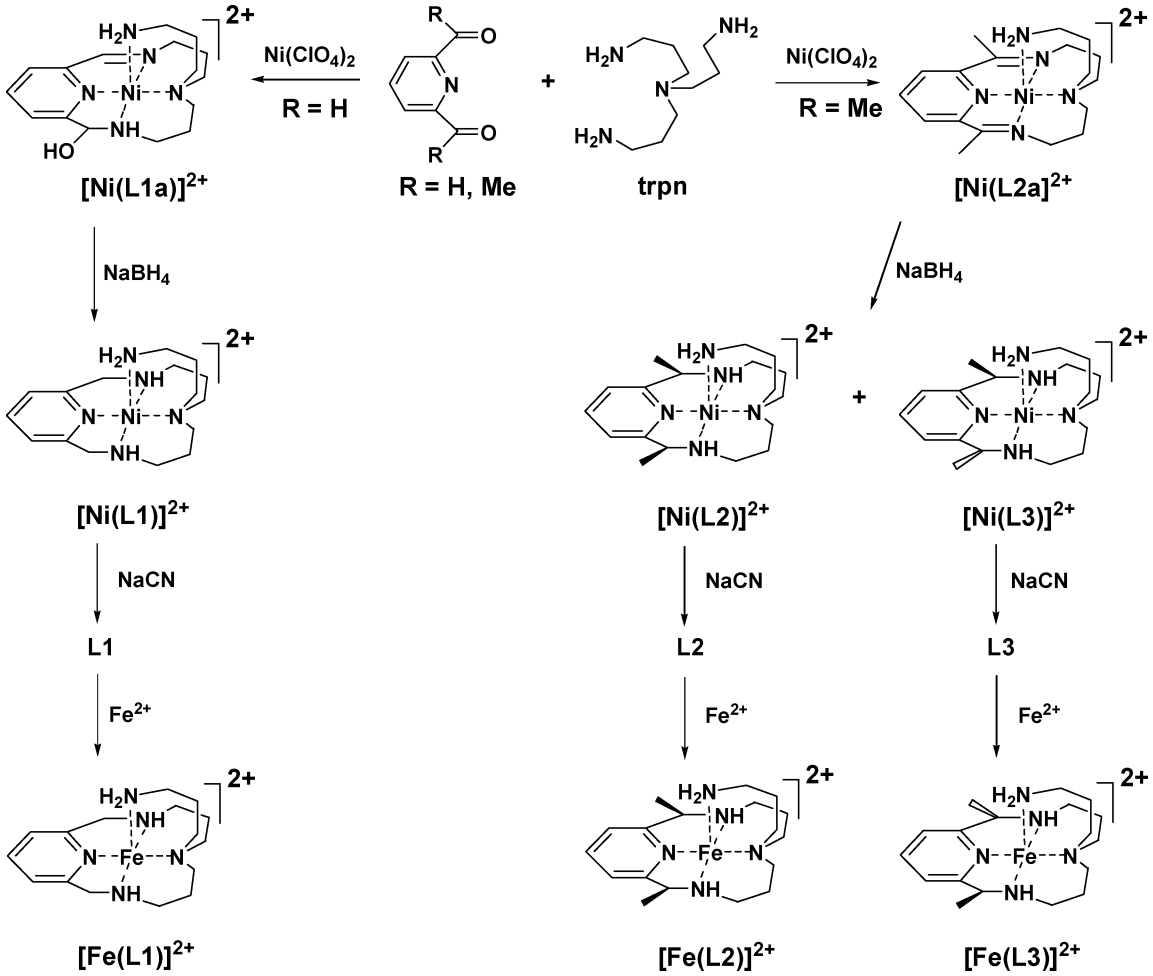

an argon atmosphere. Upon mixing, the solution turned red. Dark-red crystals were obtained after several days by vapor diffusion of diethyl ether into this solution. Yield: 81 mg (34%). ES-MS(+) (CH_3CN): *m*/*z* 467.0 ({[Fe(L5)](CF_3SO_3)}$^+$, 100%), 179.6 ({[Fe(L5)(CH_3CN)]}$^{2+}$, 22%). Anal. Calcd (found) for $C_{19}H_{29}N_5FeO_6F_6S_2$: C, 34.71 (33.92); H, 4.45 (4.84); N, 10.65 (10.08); Fe, 8.49 (8.20). ^{1}H NMR spectroscopy of a pure L5 isomer (δ, ppm in $CDCl_3$): 1.46 (6H, d), 1.69−1.81 (4H, m), 2.74−3.06 (8H, m), 3.91 (2H, quartet), 7.12 (2H, d), 7.74 (1H, t).

X-ray Diffraction Studies. Pertinent crystallographic data and experimental conditions are summarized in Table 1. Suitable crystals of **2′**, **3**, and **4** were mounted on a glass fiber using paratone oil. Data were collected using a Bruker SMART CCD (charge-coupled device) based diffractometer equipped with an LT-3 low-temperature apparatus operating at 173 K. Data were measured using ω scans of 0.3° per frame for 30 s, such that a hemisphere was collected. A total of 1650 frames were collected with a maximum resolution of 0.75 Å. For complex **4**, the first 100 frames were re-collected at the end of the data collection to monitor for decay. Cell parameters were retrieved using *SMART*[46] software and refined using *SAINT*[47] on all observed reflections. Data reduction was performed using the *SAINT* software, which corrects for Lorentz and polarization effects. For complex **3**, absorption corrections were applied using *SADABS*.[48] The structures were solved by direct method using the *SHELXS-97*[49] program and refined by the least-squares method on F^2, *SHELXL-97*,[50] incorporated in *SHELXTL V5.10*.[51] All non-hydrogen atoms were refined anisotropically. Hydrogen atoms were calculated by geometrical methods and refined as a riding model.

For complex **2′**, one perchlorate ion was found to be disordered and was modeled in two positions. Similarity restraints were applied using the SADI command. For complex **3**, one triflate ion was found to be disordered and was modeled in two positions. One of the C−N bonds on the macrocycle was found to be partially oxidized (13% in the oxidized form). To account for that, the corresponding nitrogen N2 was modeled in two positions.

Catalysis Experiments. Solutions of the iron(II) complexes were prepared under an argon atmosphere (7.2 μmol, 5% catalyst) in 1.0 mL of dry acetonitrile; various additives (i.e., triflic acid or hydrochloric acid) were added when necessary. Cyclooctene or 1-decene (0.3 mL, 0.144 mmol) premixed with nitrobenzene (internal standard, 0.058 mmol) was added to the catalyst solution using a syringe. To this mixture was added using a syringe hydrogen

(46) *SMART V 5.054 (NT). Software for the CCD Detector System*; Bruker Analytical X-ray Systems: Madison, WI, 1998.
(47) *SAINT V 6.01 (NT). Software for the CCD Detector System*; Bruker Analytical X-ray Systems: Madison, WI, 1999.
(48) *SADABS*, Program for absorption corrections using Siemens CCD based on the method of Robert Blessing: Blessing, R. H. *Acta Crystallogr*. **1995**, *A51*, 33−38.
(49) Sheldrick, G. M. *SHELXS-90, Program for the Solution of Crystal Structure*; University of Gottingen: Göttingen, Germany, 1990.
(50) Sheldrick, G. M. *SHELXL-97, Program for the Refinement of Crystal Structure*; University of Gottingen: Göttingen, Germany, 1997.
(51) *SHELXTL 5.10 (PC/NT Version). Program library for Structure Solution and Molecular Graphics*; Bruker Analytical X-ray Systems: Madison, WI, 1998.

Table 1. Crystallographic Data for **2′**, **3**, and **4**

	2′	**3**	**4**
empirical formula	$C_{18}H_{33}Cl_2FeN_5O_8$	$C_{20}H_{33}F_6FeN_5O_6S_2$	$C_{21}H_{32}F_6FeN_6O_6S_2$
formula weight (amu)	574.24	673.48	698.50
cryst habit, color	needle, colorless	plate, pale yellow	block, red
cryst syst	monoclinic	triclinic	triclinic
space group	$P2(1)/c$	$P\bar{1}$	$P\bar{1}$
a (Å)	16.485(2)	8.7638(13)	10.3970(8)
b (Å)	8.8459(11)	8.9187(13)	12.4925(12)
c (Å)	17.364(3)	19.950(3)	13.2344(10)
α (deg)	90	93.991(3)	81.333(2)
β (deg)	98.145(3)	96.393(3)	70.9660(10)
γ (deg)	90	115.802(2)	65.5250(10)
V (Å^3)	2506.6(6)	1382.9(4)	1478.7(2)
Z	4	2	2
D_c (g cm^{-3})	1.522	1.617	1.569
cryst size (mm^3)	0.09 × 0.06 × 0.05	0.18 × 0.16 × 0.06	0.20 × 0.15 × 0.10
R1 [$I > 2\sigma(I)$]	0.0912	0.0489	0.0566
wR2 (all data)	0.2784	0.1384	0.1735

peroxide (0.3 mL, 0.216 mmol, 0.72 M). The reactions were run anaerobically at room temperature, and 50 μL aliquots were taken before the addition of hydrogen peroxide and after 5 min of reaction. These aliquots were immediately diluted in 1 mL of diethyl ether, filtered, and analyzed by GC. Reaction yields and conversions reported are averages of at least two runs. Final catalyst:substrate: H_2O_2 ratio = 1:20:30.

Cyclic Voltammetry. Cyclic voltammetry measurements were carried out in a glovebox with an argon atmosphere using a CH Instruments model 830 electrochemical analyzer and a three-electrode cell (glassy carbon as the working electrode and platinum wires as the counter and reference electrodes). Dry acetonitrile with a 0.1 M [n-Bu_4N][PF_6] supporting electrolyte was used as the solvent, and the complex concentration used for electrochemical measurements was 2 mM. In additional experiments, small amounts of triflic acid or triethylamine were introduced into the complex solution. Ferrocene was used as the internal standard [$E_{1/2}$(Fc/Fc$^+$) = 0.590 V vs SHE in MeCN[42]]. In all experiments, the range of potentials was scanned with a rate of 100 mV s^{-1}.

Acid−Base Titrations. In a typical experiment, a 1 mM solution of **1** or **2** in anhydrous air-free acetonitrile was prepared under an argon atmosphere. The UV−vis cells containing 2 mL of solution were capped with a septum, and successive amounts of acid (0−1.2 equiv of triflic acid or perchloric acid in acetonitrile; the total volume added was 60 μL of a 0.04 M solution) were added using a syringe. The resulting solutions were titrated with the base (0−1.6 equiv of sodium hydroxide in water; the total volume added was 8 μL of a 0.4 M solution). UV−vis spectra were recorded on a Jasco V-570 spectrophotometer at room temperature.

Magnetic Susceptibility Measurements in Solutions. The spin states of the protonated and nonprotonated forms of complex **2** were determined using the Evans method[52−54] on a Bruker DPX-300 spectrometer, at room temperature. NMR tubes containing complex **2** (0.5 mL, 10 mM) dissolved in deuterated acetonitrile (with 1% tetramethylsilane, TMS) were prepared under an argon atmosphere. A total of 0−5 mol equiv of triflic acid was added to the sample. A sealed capillary containing the blank solvent was inserted into the NMR tubes. The shift of the TMS peak in the presence of the complex was compared to that of the TMS peak in the inner tube.

The mass susceptibility χ_p (cm^3 g^{-1}) of the dissolved iron complex was determined using the simplified eq 1,[52,53] where $\delta\nu$

$$\chi_p = 3\delta\nu/4\pi\nu_0 C M_w + \chi_0 \quad (1)$$

is the shift in frequency (Hz) from the value found for the pure solvent, C is the concentration of the complex (mol cm^{-3}), M_w is the molecular weight of the complex (g mol^{-1}), ν_0 is the operating frequency of the NMR spectrometer (Hz), and χ_0 is the mass susceptibility of the pure solvent (-0.682×10^{-6} cm^3 g^{-1} for acetonitrile). The $4\pi/3$ shape factor is for a cylindrical sample in a superconducting magnet.

The effective magnetic moment μ (T J^{-1}) can be obtained using simplified eq 2,[55] where T is the temperature (K). The number of

$$\mu^2 = 8\chi_p M_w T \quad (2)$$

unpaired electrons per molecule, n, can be easily derived from the magnetic moment using eq 3,[55] where S is the electronic spin and

$$\mu^2 = g^2 S(S+1) \quad (3)$$

g the Landé factor. This can be further simplified into $n(n+2)$ for $g = 2$.

Results

Synthesis of Complexes. Complexes **1**−**3** bearing pentadentate aminopyridine ligands were prepared under an argon atmosphere by reacting a slight excess of ligands L1−L3 dissolved in dry methanol with iron(II) triflate solutions in dry methanol or acetonitrile. As was previously reported elsewhere,[44] ligands L1−L3 were prepared by template condensation of diformylpyridine or diacetylpyridine and the tripodal tetramine trpn in the presence of nickel(II), followed by a reduction with excess sodium borohydride (Scheme 1). Treatment of the reduced nickel complexes with an excess of sodium cyanide led to the isolation of the metal-free macrocycle. In the case of diacetylpyridine derivatives, separation of the two different isomers of the ligand (the meso form L2, with the two methyl groups on the same side of the macrocycle ring, and the racemic form L3, with the

(52) Piguet, C. *J. Chem. Educ.* **1997**, *74*, 815−816.
(53) Sur, S. K. *J. Magn. Reson.* **1989**, *82*, 169−173.
(54) Evans, D. F. *J. Chem. Soc.* **1959**, 2003−2005.
(55) Girerd, J. J.; Journaux, Y. In *Physical Methods in Bioinorganic Chemistry*; Que, L., Jr., Ed.; University Science Books: Sausalito, CA, 2000; p 321−374.

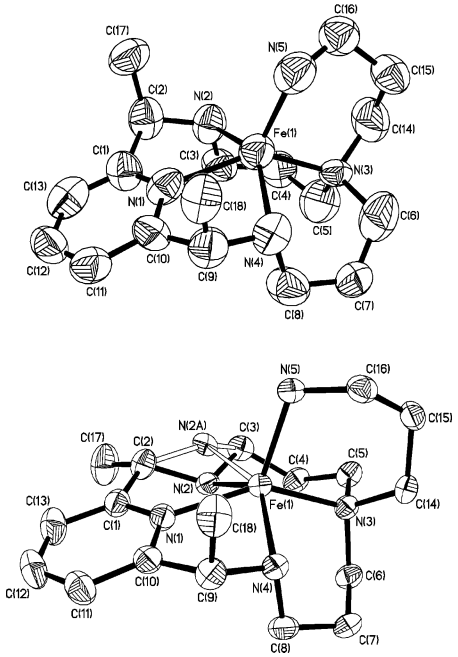

Figure 1. Representation of the X-ray structures of the complex cations in **2′** (top) and **3** (bottom), showing 50% probability thermal ellipsoids. Hydrogen atoms are not included for clarity.

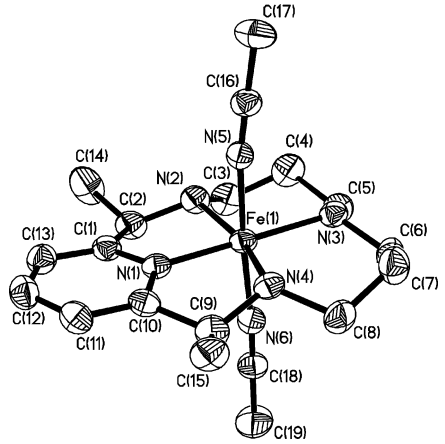

Figure 2. Representation of the X-ray structure of the complex cation in **4**, showing 50% probability thermal ellipsoids. Hydrogen atoms are not included for clarity.

Scheme 2. Reversible Protonation of the Amine on the Ligand Arm

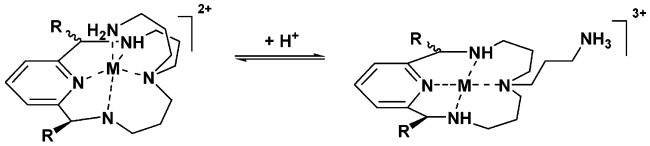

M = Ni, Cu, Fe
R = H or CH_3

two methyl groups on opposite sides) can be achieved by successive recrystallizations of the reduced nickel precursor. Pure meso isomer L2, which forms less soluble nickel(II) complexes, is easily obtained in this way. However, purification of racemic L3, which forms more soluble complexes, is material- and time-consuming.[44] For practical purposes, samples containing >80% of L3 (the balance: L2) were used in most of catalytic experiments (see below).

A similar synthetic procedure was used to prepare complexes **4** and **5** with analogous tetradentate aminopyridine ligands L4 and L5 (also referred to as CRH in the literature).[45] In this case, two isomers of the ligand are also obtained (meso form L4 and racemic form L5), which can be purified by multiple recrystallizations of the reduced nickel precursor. The iron complexes **4** and **5** were prepared under an argon atmosphere by reacting a slight excess of the ligand dissolved in dry methanol with iron(II) triflate dissolved in acetonitrile.

Structures of the Complexes. Three iron(II) complexes with pentadentate ligands L2 and L3 and a tetradentate ligand L4 were structurally characterized (Figures 1 and 2). Selected bond lengths and angles are reported in Table 2. In the case of complexes **2** and **3**, all five nitrogen atoms of the pentadentate ligands are coordinated to the iron center, resulting in a square-pyramidal geometry (Figure 1). The four nitrogen donors of the macrocyclic ring occupy the equatorial positions, and the fifth nitrogen from the pendant arm binds in the axial position. No coordination of either the solvent molecule or anions was observed. This geometry is similar to that of the nickel(II) and copper(II) analogues of these complexes.[44,56] Fe−N distances (2.06−2.22 Å) are typical of high-spin iron(II) complexes,[57] with the shortest distances to the pyridine nitrogens. These Fe−N distances are longer that those found in the nickel(II) (1.99−2.13 Å) and copper(II) (1.96−2.17 Å) analogues[44] (Table S1 in the Supporting Information), in agreement with a general trend of shortening of the M−N distances with increasing atomic numbers.[58] Iron(II) is displaced from the mean N4 plane of the macrocycle by 0.6−0.7 Å, an even more significant displacement than ca. 0.4−0.5 Å previously found for nickel(II) and copper(II) complexes with L1−L3.[44]

Unlike nickel(II) and especially copper(II), iron(II) does not have a strong structural preference for a square-pyramidal geometry (the crystal-field stabilization energy would favor low-spin octahedral complexes for a d^6 configuration). Nevertheless, this coordination mode is often imposed by hemoproteins, such as hemoglobin or myoglobin, and examples of synthetic square-pyramidal, high-spin iron(II) complexes have also been described in the literature. Closely related high-spin iron complexes with a tetradentate macrocycle CRH (L4) or tetramethylcyclam and an additional monodentate anion (Cl^-, Br^-, I^-, or N_3^-) have been reported by Busch and co-workers[59−61] to adopt this geometry on the basis of their magnetic and spectroscopic properties. A few

(56) Herrera, A. M.; Kalayda, G. V.; Disch, J. S.; Wikstrom, R. P.; Korendovych, I. V.; Staples, R. J.; Campana, C. F.; Nazarenko, A. Y.; Haas, T. E.; Rybak-Akimova, E. V. *Dalton Trans.* **2003**, 4482−4492.
(57) Simaan, J.; Poussereau, S.; Blondin, G.; Girerd, J. J.; Defaye, D.; Philouze, C.; Guilhem, J.; Tchertanov, L. *Inorg. Chim. Acta* **2000**, *299*, 221−230.
(58) Latos-Grazynski, L.; Lisowski, J.; Olmstead, M. M.; Balch, A. L. *Inorg. Chem.* **1989**, *28*, 1183−1188.
(59) Merrell, P. H.; Goedken, V. L.; Busch, D. H. *J. Am. Chem. Soc.* **1970**, *92*, 7590−7591.
(60) Riley, D. P.; Merrell, P. H.; Stone, J. A.; Busch, D. H. *Inorg. Chem.* **1975**, *14*, 490−494.
(61) Hodges, K. D.; Wollmann, R. G.; Barefield, E. K.; Hendrickson, D. N. *Inorg. Chem.* **1977**, *16*, 2746−2751.

Table 2. Selected Bond Lengths (Å) and Angles (deg) for **2′**, **3**, and **4**

	2′	**3**	**4**
Fe(1)−N(1)	2.092(6)	2.096(3)	1.886(2)
Fe(1)−N(2)	2.163(6)	2.182(3)	2.027(2)
Fe(1)−N(3)	2.129(5)	2.122(3)	2.037(2)
Fe(1)−N(4)	2.224(6)	2.183(3)	2.023(2)
Fe(1)−N(5)	2.070(7)	2.063(2)	1.933(2)
Fe(1)−N(6)			1.924(2)
N(1)−Fe(1)−N(2)	77.1(2)	73.86(11)	82.57(9)
N(1)−Fe(1)−N(3)	140.3(2)	146.70(9)	179.60(8)
N(1)−Fe(1)−N(4)	76.0(2)	75.29(10)	81.70(9)
N(1)−Fe(1)−N(5)	122.8(2)	118.43(10)	93.34(9)
N(1)−Fe(1)−N(6)			89.77(9)
N(2)−Fe(1)−N(3)	93.5(2)	93.32(11)	97.17(9)
N(2)−Fe(1)−N(4)	145.2(2)	132.29(12)	163.30(10)
N(2)−Fe(1)−N(5)	111.5(3)	114.00(13)	88.03(9)
N(2)−Fe(1)−N(6)			93.08(9)
N(3)−Fe(1)−N(4)	93.28(19)	93.00(9)	98.53(9)
N(3)−Fe(1)−N(5)	96.7(2)	94.87(10)	86.35(9)
N(3)−Fe(1)−N(6)			90.55(9)
N(4)−Fe(1)−N(5)	101.5(2)	112.47(10)	87.32(9)
N(4)−Fe(1)−N(6)			92.43(9)
N(5)−Fe(1)−N(6)			176.82(9)
metal displacement from the N(1)−N(2)−N(3)−N(4) mean plane	0.6406 (0.0031)	0.7024 (0.0015)	0.0519 (0.0011)

structurally characterized high-spin iron(II) porphyrin complexes have been found to also adopt a square-pyramidal geometry, with four equatorial nitrogen donors from the porphyrin ring and a chloride in the fifth axial position.[58] Other examples are provided by amide-containing models of BLM, such as PMAH.[28]

To our knowledge, complexes **2** and **3** are the first structurally characterized high-spin iron(II) complexes bearing pentadentate aminopyridine ligands that adopt a square-pyramidal geometry. High-spin iron(II) complexes with pentadentate aminopyridine ligands usually adopt a classic octahedral geometry, with five nitrogen atoms provided by the pentadentate ligand and one additional site occupied by an external monodentate ligand X, usually a chloride (X = Cl^-,[31,33−35,37,42] Br^-,[33] OBz^-, H_2O, MeOH[42]). In many cases, a change in the solvent[35] or in the nature of the axial ligand (to X = pyridine, CN^-,[42] MeCN,[40] or NCS^- [31]) results in a spin-state change. In our case, a large displacement of iron from the macrocyclic plane toward the coordinated amino group in the pendant arm prevents the coordination of additional ligands in the trans position.

The crystal structure of complex **4**, containing the meso form of the tetradentate ligand CRH (L4), reveals a distorted octahedral geometry around the iron(II) center, with four equatorial nitrogen donors from the aminopyridine ligand and two nitrogen-bound acetonitriles in the axial positions (Figure 2). Fe−N distances (1.89−2.04 Å) are typical of low-spin iron(II) complexes,[57] with the shortest contact with the pyridine nitrogen. Although several Fe^{II}CRH complexes were previously prepared and spectroscopically characterized in detail,[59,60] complex **4** is the first Fe^{II}CRH complex that is structurally characterized. One Fe^{III}(*meso*-CRH) structure, however, has been reported, which revealed an octahedral iron center with a folded macrocycle and two chloride anions in cis positions.[62] Crystal structures of Ni^{II}- and Cu^{II}(*meso*-CRH) showed different possible geometries around the metal center: planar[63] and octahedral[64,65] geometries were observed with nickel, whereas square-pyramidal structures with one chloride in the axial position were favored with copper.[66,67] Folding of the macrocycle was observed when an additional bidentate ligand (ethylenediamine) was present.[64,68] The only crystallographically characterized complex with racemic CRH as a ligand contained square-planar nickel(II).[69]

Pendent Arm Protonation Equilibria. In the nickel(II) and copper(II) complexes with pentadentate pyridine containing macrocycles $[M(L1)]^{2+}$−$[M(L3)]^{2+}$ (M = Cu, Ni), reversible protonation of the aminopropyl pendant arm was observed upon a change of the pH (Scheme 2).[44] Detailed acid−base titrations were performed in an aqueous solution, revealing that protonation of the arm occurs under mild conditions ($pK_a \approx 6-8$). In addition to characteristic reversible changes in UV−vis and EPR spectra, one crystal structure of the protonated form of the $[Cu(H\text{-}L2)]^{3+}$ complex was reported, showing a change in the geometry from five-coordinate square-pyramidal to essentially four-coordinate square-planar copper(II), with a weakly bound axial acetonitrile molecule on the opposite side of the macrocycle with

(62) Cairns, C. J.; Heckman, R. A.; Melnyk, A. C.; Davis, W. M.; Busch, D. H. *J. Chem. Soc., Dalton Trans.* **1987**, 2505−2510.
(63) Drew, M. G. B.; Hollis, S. *Acta Crystallogr., Sect. B* **1980**, *36*, 718−720.
(64) Drew, M. G. B.; Hollis, S. *Acta Crystallogr., Sect. B* **1980**, *36*, 2629−2632.
(65) Drew, M. G. B.; Hollis, S. *Acta Crystallogr., Sect. B* **1980**, *36*, 1944−1947.
(66) Caira, M. R.; Nassimbeni, L. R.; Woolley, P. R. *Acta Crystallogr., Sect. B* **1975**, *31*, 1334−1338.
(67) Lindoy, L. F.; Rambusch, T.; Skelton, B. W.; White, A. H. *Dalton Trans.* **2001**, 1857−1862.
(68) Drew, M. G. B.; Rice, D. A.; Binsilong, S.; Yates, P. C. *J. Chem. Soc., Dalton Trans.* **1986**, 1081−1086.
(69) Dewar, R.; Fleische, E. *Nature* **1969**, *222*, 372−373.

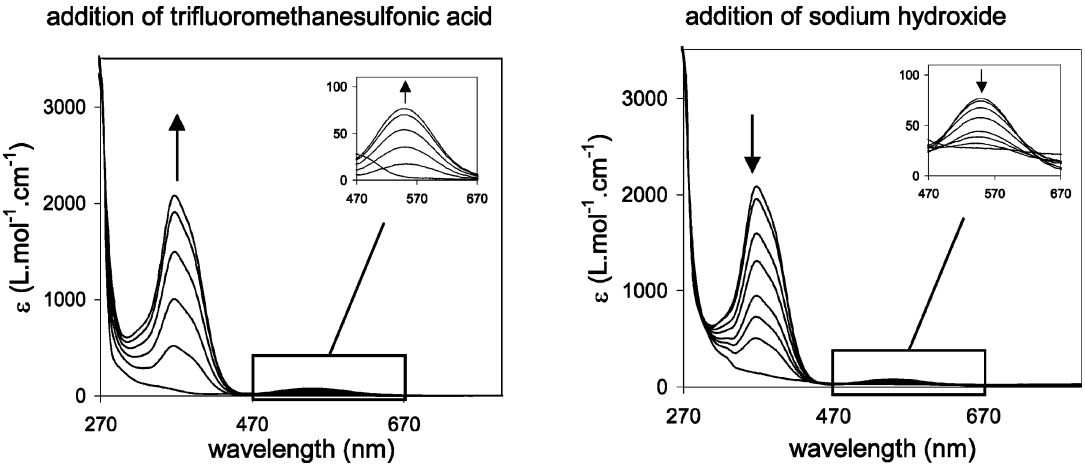

Figure 3. Spectral changes upon (a) successive addition of 0−1.0 equiv of triflic acid to **2** (1 mM in acetonitrile, room temperature, under an argon atmosphere) followed by (b) successive addition of 0−1.4 equiv of sodium hydroxide. Insets show expansions of the 470−670 nm region.

respect to the uncoordinated protonated pendant arm.[44] In contrast to the reversible protonation of modified macrocycles, full destruction of the complexes due to protonation of multiple donor atoms with an excess of acid is usually observed for complexes of acyclic polyamines.[70]

Reversible protonation of the ligand arm of L1−L3 can be achieved in the iron(II) complexes **1**−**3** and was observed spectrophotometrically. This phenomenon was not previously reported for non-porphyrin iron complexes. The UV−vis spectra of complexes **1**−**3** in acetonitrile are featureless in the visible region and contain an intense UV band below 300 nm corresponding to the pyridine $\pi-\pi^*$ transition. The addition of noncoordinating acids [e.g., triflic acid (Figure 3) or perchloric acid (Figure S1 in the Supporting Information)] to the solutions of complex **2** resulted in a small increase in the absorbance in the visible region at $\lambda = 545$ nm (final $\epsilon = 80$ L mol^{-1} cm^{-1}) and in a large increase in the near-UV region at $\lambda = 367$ nm (final $\epsilon = 2090$ L mol^{-1} cm^{-1}) with a shoulder at 387 nm (final $\epsilon = 1465$ L mol^{-1} cm^{-1}). The absorbance changes level off when an excess of acid is added. Upon the addition of a base, the reverse spectral changes were observed and the final spectrum is similar to that of the starting material, showing the reversibility of this acid−base process. Titration with an acid or a base can be repeated several times without decomposition of the macrocycle. Nonmethylated complex **1** demonstrated a similar behavior (Figure S2 in the Supporting Information).

Evidence that a singly protonated species is formed upon the addition of acid was obtained by electrospray ionization mass spectrometry (ESI-MS), which showed in all cases new peaks that could be assigned to the protonated form of the complex (e.g., at *m*/*z* 262.6 consistent with $\{[Fe(L2\text{-}H)](CF_3SO_3)\}^{2+}$ and at *m*/*z* 673.9 consistent with $\{[Fe(L2\text{-}H)](CF_3SO_3)_2\}^{+}$ for **2** + HTf).

Interestingly, the addition of 1−2 equiv of HCl to **2** did not result in any spectral change in the visible region (Figure S4 in the Supporting Information). This observation can be explained by the fact that, in the presence of coordinating anions like chlorides, the coordination geometry of iron remains essentially unchanged due to coordination of the chloride anion instead of the amino group of the ligand arm. Evidence for the protonation of the ligand arm and coordination of the chloride ions was also obtained by ESI-MS (Figure S4 in the Supporting Information).

The UV−vis spectrum of the iron(II) complex with a tetradentate macrocycle L4 (Figure S3 in the Supporting Information) contains intense absorption bands in the near-UV region [$\lambda_{max} = 370$ nm (sh) ($\epsilon = 2660$ L mol^{-1} cm^{-1}) and 390 nm ($\epsilon = 3120$ L mol^{-1} cm^{-1})] and a much less intense absorption band in the visible region [$\lambda_{max} = 526$ nm ($\epsilon = 120$ L mol^{-1} cm^{-1})]. The high similarity between the UV−vis spectra of the protonated forms of complexes **1**−**3** (obtained in the presence of triflic acid) and the spectrum of **4** (Figure S3 in the Supporting Information) is indicative of similar coordination environments and spin states of iron(II) and confirms that the macrocyclic complex remains intact in the presence of acid. The spectral changes observed upon the addition of triflic acid to complexes **1**−**3**, with an increase in the absorbance in the visible region at $\lambda = 540-545$ nm (final $\epsilon = 80-125$ L mol^{-1} cm^{-1}) and in the UV region at $\lambda = 361-367$ nm (final $\epsilon = 2090-2480$ L mol^{-1} cm^{-1}), are typical of high-spin to low-spin transformations.[31,35,42] This spin state change was confirmed by magnetic susceptibility measurements.

Magnetic Properties. Magnetic susceptibility measurements using Evans' method were performed on acetonitrile solutions of complexes **2** and **4** both in the presence and in the absence of triflic acid. The effective magnetic moment obtained for complex **2** ($\mu = 5.15\ \mu_B$) is characteristic of high-spin iron(II) systems and is very close to the published values for the solid five-coordinate, high-spin Fe^{II}CRH analogues (Table 3). In the presence of triflic acid, the observed effective magnetic moment significantly decreases ($\mu = 3.03\ \mu_B$), although paramagnetism does not vanish, as would be expected for low-spin iron(II) systems. Adding excess acid does not cause further changes in the effective magnetic moment of **2** in solution. As a control, a low-spin complex **4**, bearing the tetradentate ligand CRH and two axial

(70) Ackermann, H.; Prue, J. E.; Schwarzenbach, G. *Nature* **1949**, *163*, 723.

Table 3. ^{1}H NMR Shifts of the Internal Standard (TMS), Magnetic Susceptibility, and Effective Magnetic Moments of Iron(II) Macrocyclic Complexes

complex	$\delta\nu$ (Hz)	$\chi_p \times 10^6$ (cm^3 g^{-1})	μ (T J^{-1})	spin state	ref
complex **2**[a]	147.9	16.8	5.15	hs	this work
complex **2** with 1−2 equiv of HOTf[a]	55.1	5.8	3.03	hs−ls equilibrium	this work
complex **4**[a]	0	0	0	ls	this work
[Fe(CRH)Cl]Cl[b]			5.20	hs	59
[Fe(CRH)Br]Br[b]			5.11	hs	59
[Fe(CRH)I]I[b]			5.05	hs	59
[Fe(CRH)(NCS)$_2$][b]			0.8	ls	60

[a] Obtained at room temperature using the Evans method (10 mM in MeCN). [b] Obtained at room temperature using the Faraday technique (~1 mM in MeOH).

Table 4. Redox Potentials of Ferrous Complexes Studied ($E_{1/2}$[Fc/Fc$^+$] = 0.17 vs SCE, 0.59 V vs SHE in Acetonitrile)

entry	complex	additive	$E_{1/2}$ adjusted vs Fc/Fc$^+$ (V)	$E_{1/2}$ adjusted vs SCE (V)	$E_{1/2}$ adjusted vs SHE (V)	ΔE_p (V)	wave	reversibility[b]
				Pentadentate				
1	**1**		0.54	0.71	1.13	0.18	1	QR
							multi	IR/QR
2		1 equiv HOTf	0.53	0.70	1.12	0.17	1	QR
3	**2**		0.58	0.75	1.15	0.26	1	QR
			0.56	0.73	1.17	0.54	2	QR
4		1 equiv HOTf	0.51	0.68	1.10	0.14	1	QR
5		1 equiv Et$_3$N	0.60	0.77	1.19	0.60	1	QR
							2[a]	IR
6	**3**		0.55	0.72	1.14	0.22	1	QR
			0.55	0.72	1.14	0.51	2	IR
7		1 equiv HOTf	0.51	0.72	1.10	0.21	1	QR
				Tetradentate				
8	**4**		0.40	0.57	0.99	0.11	1	R
9		1 equiv HOTf	0.40	0.57	0.99	0.12	1	R

[a] Redox wave due to Et$_3$N. [b] R, reversible; QR, quasireversible; IR, irreversible.

acetonitriles, was investigated under the same conditions and showed no splitting of the TMS peak, indicating the absence of paramagnetic species. As expected, magnetic susceptibility of **4** did not change upon the addition of triflic acid to its acetonitrile solution.

On the basis of these observations, we propose that, upon protonation of **2**, the ligand arm dissociates from the iron center, thus liberating the fifth axial coordination site (Scheme 2). The complexes with protonated pentadentate ligands L1−L3 may bind either one or two acetonitrile molecules. The former case may result in a high-spin configuration of iron(II), while the latter coordination mode stabilizes a low-spin configuration of iron(II) (as shown by the X-ray structure and magnetic susceptibility of [Fe(L4)-$(CH_3CN)_2]^{2+}$). An equilibrium between [Fe(H-L2)$(CH_3$-$CN)]^{3+}$ and [Fe(H-L2)$(CH_3CN)_2]^{3+}$ results in intermediate values of the effective magnetic moment in an acetonitrile solution of the protonated complex **2**. The pendant arm, even in its protonated form, may create steric hindrance for additional axial ligand binding, thus destabilizing a low-spin, six-coordinate form of [Fe(H-L2)$(CH_3CN)_2]^{3+}$ as compared to the analogous low-spin complex **4** with a tetradentate ligand, [Fe(L4)$(CH_3CN)_2]^{2+}$. In the solid state, complex **4** is also able to lose one acetonitrile, as evidenced by the color change from red crystals to green powder observed upon drying.[71]

(71) The experimental data can also be interpreted in terms of an intermediate-spin iron(II) configuration.

Electrochemistry. CVs of complexes **1**−**3** in acetonitrile always showed one pronounced quasi-reversible wave around $E_{1/2}$ = 0.53 V vs Fc$^+$/Fc ($\Delta E_p \approx$ 220 mV) and at least one additional less pronounced wave of similar potential but larger peak-to-peak separation ($\Delta E_p \approx$ 530 mV; Table 4). The redox potentials observed are slightly larger than those of other iron(II) complexes of pentadentate aminopyridine ligands.[34,42] Figure 4 shows the CV of complex **2** where clearly two redox processes are observed ($E_{1/2}$ = 0.58−0.56 V with ΔE_{p1} = 260 mV and ΔE_{p2} = 540 mV). Similar CVs were obtained for complexes **1** and **3** (Figures S5 and S6 in the Supporting Information). In these systems, it is likely that the two forms of the iron complex (arm-on, five-coordinate and arm-off, six-coordinate) coexist in a neutral solution, giving rise to two waves in the CV. This ligand protonation equilibrium was directly observed by UV−vis for the reduced form of the complexes.

In order to confirm this hypothesis, cyclic voltammetry of **2** with the addition of triflic acid (which quantitatively protonates the aminopropyl arm in **2**; see Figure 3) or triethylamine (which reverses this process) was performed under the same conditions (Figures S7 and S8 in the Supporting Information). In the presence of an acid, the redox wave with a larger peak separation disappeared and only one quasi-reversible wave was observed at $E_{1/2}$ = 0.51 V vs Fc$^+$/Fc (ΔE_p = 140 mV), indicating the presence of only one form of complex **2**. The opposite effect was observed in the presence of a base: the quasi-reversible wave with a smaller

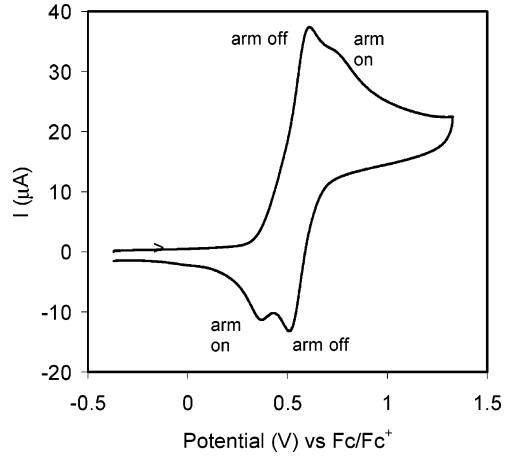

Figure 4. CV of complex **2** (2 mM in MeCN with 0.1 M [n-Bu_4N][PF_6] as the supporting electrolyte, under an argon atmosphere; scan rate 100 mV s^{-1}).

peak separation disappeared and the only quasi-reversible wave observed had $E_{1/2} = 0.60$ V vs Fc/Fc^+ ($\Delta E_p = 600$ mV), which clearly indicates the sole presence of the deprotonated, five-coordinate form of complex **2**. Similar changes in CVs were observed with the other two complexes of the pentadentate ligands, **1** and **3**, in the presence of triflic acid. It is interesting to note the large difference in the electron-transfer rates between the two forms, with the five-coordinate form undergoing much slower redox changes (as judged by the larger peak-to-peak separation in the CV). In this case, significant rearrangement is expected in the course of oxidation because an iron(III) complex will likely be six-coordinate and low-spin, while an iron(II) form is five-coordinate and high-spin.

Cyclic voltammetry of complex **4** showed a classic reversible wave at $E_{1/2} = 0.40$ V vs Fc^+/Fc ($\Delta E_p = 110$ V). The addition of triflic acid in that case did not result in any changes.

Catalytic Olefin Epoxidation. Catalytic epoxidation of cyclooctene and 1-decene with complexes **1**−**5** using hydrogen peroxide as the oxidant was examined in the presence and in the absence of additives. Reactions were carried out under an argon atmosphere at 25 °C. The goal of these experiments was to compare the relative effectiveness of several structurally related complexes in the catalytic formation of epoxides from olefins under mild conditions. Cyclooctene is commonly used as a good substrate for catalyst screening;[3] terminal olefins, such as 1-decene, are more challenging substrates, although they can be epoxidized with H_2O_2 in the presence of non-heme iron catalysts.[72] Tables 5 and 6 show epoxide yields after 5 min of reaction at room temperature with aminopyridine macrocyclic complexes as catalysts.

Complexes **1**−**3** bearing pentadentate aminopyridine ligands L1−L3 were found to efficiently catalyze olefin epoxidation in the presence of triflic acid (Tables 5 and 6). Epoxide yields of 66−89% with 90−98% selectivity were obtained with cyclooctene in the presence of 5 equiv of triflic acid versus

(72) White, M. C.; Doyle, A. G.; Jacobsen, E. N. *J. Am. Chem. Soc.* **2001**, *123*, 7194−7195.

Table 5. Cyclooctene Epoxidation Reaction with Hydrogen Peroxide (Final Catalyst:Substrate:H_2O_2 Ratio = 1:20:30)

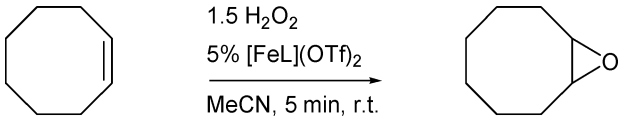

entry	catalyst	additive	epoxide yield[a] (%)	TON	convn[b] (%)	selectivity[c] (%)
			Pentadentate			
1	**1**		4	0.8	8	50
2		5 equiv HOTf	66	13.2	73	90
3	**2**		9	1.8	16	56
4		1 equiv HOTf	39	7.8	51	76
5		2 equiv HOTf	70[d]	14.0[d]	76[d]	92[d]
6		5 equiv HOTf	86	17.2	89	97
7		1.8 equiv HCl	8	1.6[d]	11[d]	73
8	**3**		6	1.2	10	60
9		5 equiv HOTf	89	19.6	91	98
10		1.8 equiv HCl	8	1.6[d]	12[d]	67
			Tetradentate			
11	**4**		32	6.4	43	74
12		1 equiv HOTf	46	9.2	54	85
13		5 equiv HOTf	67	13.4	73	92
14		1.8 equiv HCl	32	6.4	37	86
15	**5**		18	3.6	30	60
16		1 equiv HOTf	34	6.8	43	79
17		5 equiv HOTf	34	6.8	44	77
18		1.8 equiv HCl	26	5.2	33	79

[a] GC yield. [b] Internal standard used: nitrobenzene. [c] Selectivity = GC yield/conversion. [d] Two runs only.

the iron complex. No cyclooctane-1,2-diol or allylic oxidation products were detected. Slightly lower yields, ranging from 32 to 76%, were obtained with a terminal olefin, 1-decene, with 68−84% selectivity of epoxide formation. In this case, 3−6% of diol (with respect to olefin) were also formed, along with traces (<1%) of allylic alcohol. Controlled experiments showed that epoxide is stable and does not produce diol under the conditions that were used in olefin oxidation. Additions of noncoordinating acids other than triflic acid (e.g., perchloric acid) were also effective in promoting the catalytic activity of complexes **1**−**3**. Smaller amounts of triflic acid still enhanced the catalytic properties of these systems, although to a lesser extent. While 1 equiv of acid was sufficient to increase the epoxide yield from nearly 0% to a respectable 39% (Table 5), an additional 1 equiv of acid nearly doubled the epoxide yield, but a further increase in the amount of added acid caused only minor improvements, and no increase in the epoxide yield was observed when the amount of acid exceeded 5 equiv. In the absence of additives or in the presence of coordinating acids like HCl, complexes **1**−**3** did not catalyze epoxidation reactions. These results suggest that the high-spin, five-coordinate forms of complexes **1**−**3** do not promote epoxidation reactions, whereas their protonated forms are highly catalytically active.

Complexes **4** and **5**, with the analogous tetradentate macrocycle CRH, catalyze epoxidation reactions to a smaller extent. Yields of 18−32% (60−74% selectivity) with cyclooctene and yields of 18−20% (51−61%) with 1-decene were obtained under the same conditions as those discussed above for the pentadentate ligands. Identified side products include diol (up to 10% with respect to 1-decene) and traces

Table 6. 1-Decene Epoxidation Reaction with Hydrogen Peroxide (Final Catalyst:Substrate:H_2O_2 Ratio = 1:20:30)

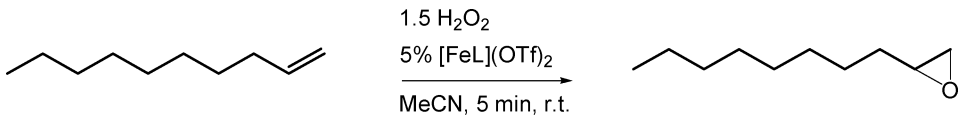

entry	catalyst	additive	epoxide yield[a] (%)	TON	convn[b] (%)	selectivity[c] (%)
			Pentadentate			
1	**1**		1	0.2	8	13
2		5 equiv HOTf	32	6.4	47	68
3	**2**		7	1.4	19	37
4		5 equiv HOTf	64	12.8	81	79
5		5 equiv $HClO_4$	46[d]	9.2[d]	68[d]	68[d]
6	**3**		4	0.8	14	29
7		5 equiv HOTf	76	15.2	91	84
			Tetradentate			
8	**4**		20	4	33	61
9		5 equiv HOTf	26	5.2	56	47
10	**5**		18	3.6	35	51
11		5 equiv HOTf	13	2.6	51	25

[a] GC yield. [b] Internal standard used: nitrobenzene. [c] Selectivity = GC yield/conversion. [d] Two runs only.

(ca. 1%) of allylic alcohol; other side products, which had significantly larger retention time, were not identified in this work. The addition of 5 equiv of triflic acid to complexes **4** and **5** also enhanced epoxide yields, but the effect is less dramatic than that with complexes **1**−**3**. This observation suggests that the role of acid is not limited to the protonation of the pendant arm. The addition of hydrochloric acid did not enhance the reactivity of complexes **4** and **5**.

Lower than 100% conversions of olefins in our experiments (Tables 5 and 6) cannot be attributed to unproductive H_2O_2 decomposition. Even though an iron(III) complex with L4 is a known catalyst for H_2O_2 decomposition,[62,73] hydrogen peroxide was not a limiting reactant under our experimental conditions. The conversions of cyclooctene and, especially, 1-decene were significantly lower when 1 equiv of H_2O_2 with respect to olefin was used and increased to the values shown in Tables 5 and 6 for 1.5 equiv of H_2O_2. However, a further increase in the amount of H_2O_2 (up to 5 equiv) did not result in additional improvements in epoxide yields or olefin conversions. Larger excesses of H_2O_2 had to be avoided because of irreversible oxidation of the ligands that deactivated the catalysts. Irreversible oxidation of the ligands was also observed upon H_2O_2 addition to complexes **1**−**5** in the absence of substrates and yielded catalytically inactive iron-containing products that were not identified in this study.

The presence of methyl substituents in the macrocyclic rings or their orientation (when meso and racemic forms of the ligands were compared) did not have a pronounced effect on epoxidation yields or selectivity.

Discussion

A detailed understanding of the structure−activity relationships in catalytic oxidations, including olefin epoxidation, was accomplished for iron hemes, where high-valent metal−oxo intermediates are usually implicated.[74−78] Oxygen binding[79] as well as oxygen and peroxide activation with heme enzymes can be dramatically enhanced by coordination of a monodentate electron-donating axial ligand to the metal center ("push effect").[80] There is also growing evidence of axial ligand effects on the reactivity of high-valent iron−oxo intermediates in synthetic porphyrin systems.[81−83] The electronic effects of additional ligands in heme chemistry are not complicated by structural reorganization: rigid porphyrins enforce tetragonal symmetry of hemes and invariably result in the trans orientation of the coordinated oxygen donor and the additional monodentate "electron-pushing" ligand. Axial coordination often changes the spin state of iron in porphyrin complexes from high spin in the five-coordinate hemes to low-spin in the corresponding six-coordinate species (e.g., complexes with a superoxide or peroxide bound trans to histidine).[84]

While in heme systems coordination of the fifth ligand to the iron center usually favors catalytic oxidations, the role of additional donor atoms in non-heme iron complexes is not well-understood.[85,86] By analogy with heme chemistry, it can be expected that five-coordinate, square-pyramidal iron

(73) Melnyk, A. C.; Kildahl, N. K.; Rendina, A. R.; Busch, D. H. *J. Am. Chem. Soc.* **1979**, *101*, 3232−3240.
(74) Meunier, B. *Chem. Rev.* **1992**, *92*, 1411−1456.
(75) Mansuy, D. *Pure Appl. Chem.* **1987**, *59*, 759−770.
(76) Dolphin, D.; Traylor, T. G.; Xie, L. Y. *Acc. Chem. Res.* **1997**, *30*, 251−259.
(77) Collman, J. P.; Zhang, X.; Lee, V. J.; Uffelman, E. S.; Brauman, J. I. *Science* **1993**, *261*, 1404−1411.
(78) McLain, J. M.; Lee, J. H.; Groves, J. T. In *Biomimetic Oxidations Catalyzed by Transition Metal Complexes*; Meunier, B., Ed.; Imperial College Press: London, 2000; pp 91−169.
(79) Momenteau, M.; Reed, C. A. *Chem. Rev.* **2004**, *94*, 659−698.
(80) Sono, M.; Roach, M. P.; Coulter, E. D.; Dawson, J. H. *Chem. Rev.* **1996**, *96*, 2841−2888.
(81) Nam, W.; Lim, M. H.; Oh, S. Y.; Lee, J. H.; Lee, H. J.; Woo, S. K.; Kim, C.; Shin, W. *Angew. Chem., Int. Ed.* **2000**, *39*, 3646−3649.
(82) Song, W. J.; Ryu, Y. O.; Song, R.; Nam, W. *J. Biol. Inorg. Chem.* **2005**, *10*, 294−304.
(83) Kamachi, T.; Kouno, T.; Nam, W.; Yoshizawa, K. *J. Inorg. Biochem.* **2006**, *100*, 751−754.
(84) Jameson, G. B.; Ibers, J. A. In *Bioinorganic Chemistry*; Bertini, I., Gray, H. B., Lippard, S. J., Valentine, J. S., Eds.; University Science Books: Sausalito, CA, 1994; pp 167−252.
(85) Tanase, S.; Bouwman, E. In *Advances in Inorganic Chemistry*; van Eldik, R., Reedijk, J., Eds.; Academic Press: Amsterdam, The Netherlands, 2006; Vol. 58, pp 29−75.

complexes with pentadentate ligands would be most active with respect to oxygen and peroxide activation. The situation is more complicated, however, in part because multiple reaction pathways are possible. After the initial coordination of hydroperoxide to the iron center, the resulting $Fe^{III}OOH$ intermediate may directly transfer an oxygen atom to olefins (in this case, iron(III) acts as a Lewis acid, activating hydroperoxide similarly to high-valent early transition metals), but it may also undergo homolytic or heterolytic cleavage, yielding Fe^{IV}═O species and hydroxyl radicals or yet-to-be observed iron(V) oxidants, respectively.[3] Iron(IV), which is a stronger Lewis acid than iron(III), may also coordinate an additional molecule of the oxidant, generating catalytically active species.[87]

For iron bleomycin, a "porphyrin-like" natural non-heme oxygen and peroxide activating system, a square-pyramidal, five-coordinate complex is believed to be reactive with oxygen or hydrogen peroxide (Chart 1).[13,88] Fe^{II}BLM is high-spin and contains an iron(II) center surrounded by four in-plane nitrogen donors, an axial primary amino group, and a labile, exchangeable oxygen donor from the sugar residue in the sixth position.[25] An oxidized form of iron bleomycin, Fe^{III}BLM, contains a low-spin, six-coordinate iron(III) center.[12] This species reacts with H_2O_2, yielding ABLM, (BLM)$Fe^{III}OOH$,[6,12] and also promotes oxidation of various substrates (e.g., ascorbate). [89] Interestingly, in acidic media, Fe^{III}BLM undergoes protonation, yielding an unreactive high-spin species (presumably, dissociation of the axial nitrogen causes this spin transition).[90] ABLM, a low-spin species with coordination geometry very similar to that of Fe^{III}BLM, is a competent oxidant in DNA strand cleavage and in other oxidations, including olefin epoxidation.[6,12] Although recent studies suggest that the FeOOH itself is the most likely reactive intermediate in oxidative DNA cleavage,[13] the detailed mechanism of olefin expoxidation[8,14,15] with ABLM was not established, and probing the role of the axial amino group coordination in the catalytic activity of FeBLM would be difficult.

The experimental data on catalytic oxidations with synthetic biomimetic non-heme iron complexes are still limited and show somewhat conflicting trends in the relative reactivity of four- and five-coordinate complexes (weakly bound solvent molecules are not taken into account).[85,91] Recent results on the formation of Fe^{IV}═O species (possible reactive intermediates in catalytic oxidations) via O−O bond homolysis in coordinated alkyl peroxides definitively demonstrated a strong, favorable push effect of an additional ligand binding.[92,93] However, the reactivity of Fe^{IV}═O with some substrates increased in the presence of coordinating anions,[94,95] while the reactivity with other substrates decreased upon anion coordination in the fifth position.[94] Furthermore, Fe^{IV}═O species are not always active in olefin epoxidation,[87] and other reactive intermediates were also proposed,[96,97] which may require two cis-positioned labile sites at the iron center: a range of iron(II) complexes with tetradentate aminopyridine ligands catalyzes olefin epoxidation or cis dihydroxylation with H_2O_2, but a complex with analogous pentadentate ligand N4py is inactive in olefin oxidations.[91,98] Other factors that influence the outcome of catalytic oxidations include ligand topology[99] and the spin state of the iron.[96] It is clear that additional studies are required in order to establish structure−activity correlations for relatively flexible polydentate aminopyridine ligands that support biomimetic oxidations with iron complexes.

Control of the geometry around iron(II) centers is often difficult because of the coordinative versatility of the metal. The design of macrocyclic ligands L1−L3 (Chart 2) addresses this problem by enforcing a square-pyramidal geometry around iron(II) centers. Equatorial coordination in these systems is constrained by the ring, which consists of a pyridine, two secondary amines, and one tertiary amine. The aminopropyl pendant arm is flexible, and its coordination in the axial position can be tuned by simple acid−base addition. The macrocycles L1−L3 contain the same kinds of donor atoms that are typically present in acyclic polydentate aminopyridine ligands used in recent years for the preparation of iron oxidation catalysts.[85,91] On the other hand, the cyclic structure of the ligands L1−L3 resembles the coordination sphere of iron in a series of oxidation catalysts based on tetramine macrocycles.[87,100,101] Tetraaza macrocycles are also among very few ligands that support well-characterized Fe^{IV} and Fe^{IV}═O moieties.[102,103] Incorporating a pyridine ring in the macrocyclic platform was previously shown to yield iron(III) complexes that were excellent catalysts for

(86) Kryatov, S. V.; Rybak-Akimova, E. V.; Schindler, S. *Chem. Rev.* **2005**, *105*, 2175−2226.
(87) Suh, Y.; Seo, M. S.; Kim, K. M.; Kim, Y. S.; Jang, H. G.; Tosha, T.; Kitagawa, T.; Kim, J.; Nam, W. *J. Inorg. Biochem.* **2006**, *100*, 627−633.
(88) Neeze, F.; Zaleski, J. M.; Zaleski, K. L.; Solomon, E. I. *J. Am. Chem. Soc.* **2000**, *122*, 11703−11724.
(89) Li, W.; Antholine, W. E.; Petering, D. H. *J. Inorg. Biochem.* **2002**, *90*, 8−17.
(90) Petering, D. H.; Mao, Q.; Li, W.; DeRose, E.; Antholine, W. E. In *Metal Ions in Biological Systems*; Sigel, A., Sigel, H., Eds.; Marcel Dekker: New York, 1996; Vol. 33, pp 619−648.
(91) Shan, X.; Que, L., Jr. *J. Inorg. Biochem.* **2006**, *100*, 421−433.
(92) Kaizer, J.; Costas, M.; Que, L., Jr. *Angew. Chem., Int. Ed.* **2003**, *42*, 3671−3673.
(93) Bukowski, M. R.; Koehntop, K. D.; Stubna, A.; Bominaar, E. L.; Halfen, J. A.; Münck, E.; Nam, W.; Que, L., Jr. *Science* **2005**, *210*, 1000−1002.
(94) Sastri, C. V.; Park, M. J.; Ohta, T.; Jackson, T. A.; Stubna, A.; Seo, M. S.; Lee, J. H.; Kim, J.; Kitagawa, T.; Münck, E.; Que, L., Jr. *J. Am. Chem. Soc.* **2005**, *127*, 12494−12495.
(95) Rohde, J.-U.; Que, L., Jr. *Angew. Chem., Int. Ed.* **2005**, *44*, 2255−2258.
(96) Chen, K.; Costas, M.; Que, L., Jr. *Dalton Trans.* **2002**, 672−679.
(97) Fujita, M.; Costas, M.; Que, L., Jr. *J. Am. Chem. Soc.* **2003**, *125*, 9912−9913.
(98) Chen, K.; Costas, M.; Kim, J.; Tipton, A. K.; Que, L., Jr. *J. Am. Chem. Soc.* **2002**, *124*, 3026−3035.
(99) Costas, M.; Que, L., Jr. *Angew. Chem., Int. Ed.* **2002**, *41*, 2179−2181.
(100) Nam, W.; Ho, R.; Valentine, J. S. *J. Am. Chem. Soc.* **1991**, *113*, 7052−7054.
(101) Nam, W.; Kim, H. J.; Kim, S. H.; Ho, R. Y. N.; Valentine, J. S. *Inorg. Chem.* **1996**, *35*, 1045−1049.
(102) Collins, T. J.; Kostka, K. L.; Münck, E.; Uffelman, E. S. *J. Am. Chem. Soc.* **1990**, *112*, 5637−5639.
(103) Rohde, J.-U.; In, J.-H.; Lim, M. H.; Brennessel, W. W.; Bukowski, M. R.; Stubna, A.; Münck, E.; Nam, W.; Que, L., Jr. *Science* **2003**, *299*, 1037−1039.

hydrogen peroxide decomposition,[62,73,104] for the oxidation of 2,2′-azinobis(3-ethylbenzothiazoline-6-sulfonate) with H_2O_2,[105] and for peroxonitrite decomposition.[106] In the present work, we modified pyridine-containing macrocycles and demonstrated that new iron complexes with pentadentate aminopyridine ligands catalyze rapid oxygen atom transfer reactions in olefin epoxidation with hydrogen peroxide in the presence of acids. Establishing the mechanism of this reaction was beyond the scope of this work and will be accomplished in our future studies.

The design features applied to L1−L3 (the presence of a flexible coordinating arm appended to a pyridine-containing tetraaza macrocyclic platform) allowed us to reproduce the tetragonal, square-pyramidal coordination geometry of iron bleomycin (Chart 1) in a relatively simple synthetic system. While the exact nature of the equatorial donor atoms is somewhat different in $[Fe(L1-L3)]^{2+}$ compared to iron bleomycin (in particular, ligands L1−L3 lack a strongly electron-donating deprotonated amide and an imidazole nitrogen), the overall coordination environment of iron in these systems is fairly similar.

The synthetic complexes developed in this work provide insights into the reactivity of iron complexes supported by tetradentate and analogous pentadentate ligands. Efficient olefin epoxidation was observed with complexes **1**−**3** and, to a lesser extent, their analogues **4** and **5** in the presence of acid. Surprisingly, the reactivity patterns of the macrocyclic complexes did not support the beneficial role of the "push effect" in activating H_2O_2 with non-heme iron systems. To the contrary, five-coordinate complexes **1**−**3** were catalytically inactive in the absence of additives, while their four-coordinate counterparts **4** and **5** showed some activity in olefin epoxidation with H_2O_2 (Tables 5 and 6). Large out-of-plane displacement of iron(II), caused by the coordination of appended amino group and accompanying stabilization of the high-spin state, disfavors coordination of H_2O_2 in the sixth position.

In the presence of poorly coordinating acids, like triflic acid, the amino group on the pendant arm is protonated (Scheme 2), resulting in changes in the spectroscopic properties (UV−vis, ESI-MS, and magnetic susceptibility) as well as catalytic properties (high epoxide yields in the presence of triflic or perchloric acid). However, the redox potentials observed for the two forms of these complexes are very close to each other and differ only in the peak-to-peak separation. Therefore, a dramatic increase in the catalytic activity of protonated complexes **1**−**3** cannot be attributed to favorable changes in redox potentials. Notably, the spin state of the iron(II) changes upon protonation of the pendant arm: five-coordinate complexes **1**−**3** are high-spin, while the protonated complexes are predominantly low-spin (Table 3). Similar crystallographically characterized, low-spin complex **4** has two acetonitrile ligands in the axial positions (Figure 2). These spin-state changes are the opposite to the spin states of iron bleomycin, where the complex with five nitrogen donors is low-spin (and catalytically active), while the protonated Fe(BLM) becomes high-spin (and catalytically inactive).[90] The redox behavior of complexes **1**−**3** suggests that the electronic "push effect" itself does not necessarily enhance the ability of non-heme iron complexes to activate oxygen and peroxides. The spin-state changes that accompany axial coordination of the fifth nitrogen donor may be more important for productive peroxide activation.

The protonation of the amine on the ligand arm also liberates a useful coordination site of the iron for hydrogen peroxide to be properly activated for olefin epoxidation. Indeed, in the presence of HCl, the amine on the ligand arm is protonated but no epoxidation occurs as a result of coordination of chlorides instead of the ligand arm, as follows from UV−vis and ESI-MS studies. When noncoordinating acids are used, the protonated primary amino group dissociates from the iron center, and a labile solvent molecule (CH_3CN) takes its place. The metal ion, which was displaced toward the amino group in the five-coordinate complexes, moves into the macrocyclic plane. Coordination of H_2O_2 in the axial position thus becomes possible. A similar beneficial effect of noncoordinating triflate anions has been previously described with porphyrin catalysts of olefin epoxidation.[81]

The presence of triflic acid also enhanced the catalytic properties of the complexes **4** and **5**. Because no changes in the iron coordination environment occur upon acid addition to **4** and **5**, the acid must play an additional role in olefin epoxidation, where general acid catalysis is commonly observed.[3] For example, it may be necessary for electrophilic activation of (coordinated) hydrogen peroxide and/or homolytic or heterolytic cleavage of the O−O bond. It was also found earlier that complex **4** is catalytically active in H_2O_2 decomposition in slightly acidic media but becomes inactive at pH 7.2, presumably because of μ-oxo dimer formation.[73,104]

We compared the catalytic activity of complexes **1**−**3** to the activity of analogous complexes **4** and **5**, which had the same equatorial coordination environment for iron but lacked the pendant arm. In the absence of acid, **4** and **5** displayed some activity, while five-coordinate complexes **1**−**3** were completely inactive. However, the activity of **4** and **5** in the presence of triflic acid was lower than that of protonated complexes **1**−**3**. This indicates that the pendant arm in **1**−**3** might play an additional role in peroxide activation after protonation. In our case, both the presence of noncoordinating acid and the presence of the aminopropyl pendant arm seem to be required for the best catalytic olefin epoxidation results. One possible explanation for this effect would be intramolecular proton transfer between the protonated amino group in the pendant arm and the coordinated peroxide, which likely facilitates electrophilic peroxide activation and triggers olefin epoxidation (Scheme 3). This "pull effect" would be similar to a proton-coupled electron transfer observed in H_2O_2 activation with "hangman" metalloporphyrins bearing a rigidly appended carboxylate group in the vicinity of the

(104) Autzen, S.; Korth, H.-G.; de Groot, H.; Sustmann, R. *Eur. J. Org. Chem.* **2001**, 3119−3125.
(105) Zhang, X. P.; Zhang, D. L.; Busch, D. H.; van Eldik, R. *J. Chem. Soc., Dalton Trans.* **1999**, 2751−2758.
(106) Zhang, X. P.; Busch, D. H. *J. Am. Chem. Soc.* **2000**, *122*, 1229−1230.

Scheme 3. Possible Intermediate in Peroxide Activation

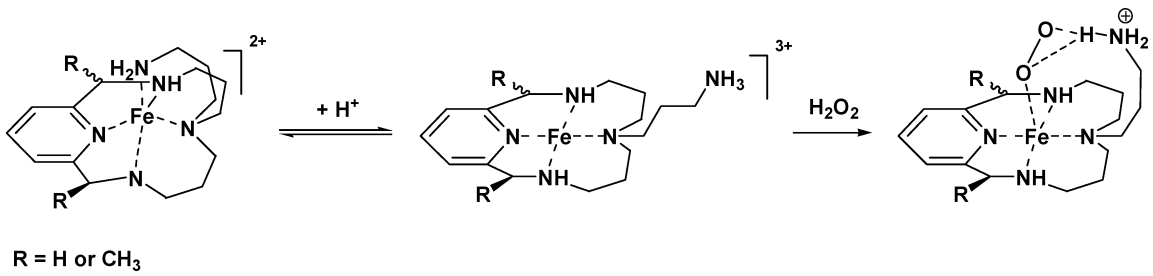

coordinated oxygen atom donor.[107,108] At present, we cannot exclude other possibilities, such as greater stability with respect to ligand oxidation of tertiary amino groups in **1**−**3** compared to secondary amino groups in **4** and **5**. Detailed studies on the mechanisms of peroxide activation with **1**−**5** and related complexes are ongoing in our laboratory.

Conclusion

In the perspective of modeling the square-pyramidal coordination geometry of iron bleomycin, a series of iron(II) complexes with pyridine-containing macrocycles were synthesized and characterized. Pentadentate ligands L1−L3, bearing an aminopropyl pendant arm, were found to bind high-spin iron(II) in a square-pyramidal geometry. Large (0.6−0.7 Å) displacement of iron from the macrocyclic plane toward the coordinating appended amino group disfavored binding of additional ligands in the sixth position. Reversible transformations between four-coordinate, square-planar and five-coordinate, tetragonal-pyramidal complexes allowed us to probe the role of iron coordination geometry in the redox reactivity of these species. In the presence of poorly coordinating acids like triflic acid, where reversible dissociation of the pendant arm occurs, these complexes efficiently catalyze olefin epoxidation using hydrogen peroxide as the oxidant, under mild conditions. Epoxide yields of 66−89% with 90−98% selectivity were obtained with cyclooctene in the presence of 5 equiv of triflic acid versus the iron complex, after 5 min at room temperature. However, in the deprotonated form or in the presence of coordinating acids like HCl, no epoxidation occurs. We conclude that five-coordinate aminopyridine macrocycles are catalytically inactive, presumably because of a large out-of-plane displacement of iron, which prevents coordination and activation of the oxidant (hydrogen peroxide). Protonation of the pendant arm causes the conversion of high-spin, five-coordinate complexes into low-spin, pseudo-octahedral species with two labile axial sites, thus greatly facilitating olefin epoxidation. These findings differ from the commonly observed enhancement of the redox reactivity due to axial ligand coordination to iron porphyrins.

Future work will focus on determining the mechanism by which these complexes activate hydrogen peroxide and examining in greater detail the role played by the amine group of the pendant arm.

Acknowledgment. The authors thank Dr. Miquel Costas and Prof. Lawrence Que, Jr. (University of Minnesota), for providing the procedure for the synthesis of iron(II) triflate and Dr. David J. Wilbur (Tufts University) for his assistance with the instrumentation methods. This work was supported by the U.S. Department of Energy—Office of Basic Energy Sciences, Grant DE-FG02-06ER15799. The CCD-based X-ray diffractometer at Tufts University was purchased through Air Force DURIP Grant F49620-01-1-0242. The NMR facility in the Chemistry Department at Tufts University was supported by NSF Grant CHE-9723772, and the ESI-MS spectrometer was funded by NSF Grant MRI 0320783.

Supporting Information Available: X-ray crystallographic data in CIF format and electronic spectra, CVs, and a table of selected bond lengths and angles. This material is available free of charge via the Internet at http://pubs.acs.org.

IC070094E

(107) Chang, C. J.; Chng, L. L.; Nocera, D. G. *J. Am. Chem. Soc.* **2003**, *125*, 1866−1876.
(108) Dempsey, J. L.; Esswein, A. J.; Manke, D. R.; Rosenthal, J.; Soper, J. D.; Nocera, D. G. *Inorg. Chem.* **2005**, *44*, 6879−6892.